Simulation of the time resolution of a 50 μm low-gain avalanche detector.

C. Peña[*,a,b], G. Deptuch[a], S. Xie[b], A. Apresyan[a], L. Narvaez[b], T. Liu[a], N. Cartiglia[c]

[a] *Fermi National Accelerator Laboratory, Batavia, IL, USA*
[b] *California Institute of Technology, Pasadena, CA, USA*
[c] *INFN, Torino, Italy*

Abstract

In this paper we report simulation results on the timing resolution of a 50 μm low-gain avalanche detector (LGAD). The simulation includes: sensor fluctuations, front-end electronics, and time quantization. Comparisons on the performance for different front-end electonics (FEE) bandwidths (BWs) are presented, as well as the dependance on singal-to-noise ratio (SNR). Two approaches to measure the timestamp are considered: leading edge (LE) and constant fraction (CF). Aditionally, the time resolution is studied as function of the irradiation of the sensor. Simulated LGAD pulses before irradiation, and after neutron fluences of 5×10^{14} n/cm^2 and 1×10^{15} n/cm^2, are studied. The time resolution a 50 μm LGADs was found to be 35 ps for FE electronics BWs larger than 350 MHz and SNRs larger than 30. The time resolution at a SNR of 30 for fluences of 5×10^{14} n/cm^2 and 1×10^{15} n/cm^2 were found to be 31 ps and 37 ps, respectively.

Key words:
Silicon, Timing, LGAD

Contents

*Corresponding author
Email address: `cmorgoth@fnal.gov` (C. Peña)

1. Introduction

LGADs are envisioned to be used in the CMS and ATLAS experiment upgrades for HL-LHC in order to overcome the event reconstruction challenges posed by the high rate of concurrent collisions per beam crossing (pileup). The implemented regions of pseudorapidity (η) are: $1.6 < |\eta| < 2.9$, and $2.4 < |\eta| < 4.2$ for CMS and ATLAS, respectively.Beam test measurements have demonstrated that the required time resolution, radiation tolerance, and uniformity of LGAD sensors can be achieved [1].

In this paper, we report simulation results on the timing resolution of a 50 μm LGAD which includes sensor fluctuations, front-end electronics (FEE) noise, and time quantization. We scan relevant parameters for timing resolution: analog bandwidths (BWs), signal-to-noise ratios (SNR), and sensor irradiation. Our results indicate that for FEE analog BWs larger than 350 MHz, corresponding to shaping times less than 1 ns, and SNR larger than 30, time resolutions of 30–37 ps and 34–47 ps are obtained when using constant fraction (CF) and leading edge (LE) discrimintators, respectively. These results are compatible with previous measurements on LGAD timing resolutions carried out under laboratory and beam test conditions [1–3]. We study the time resolution of four different FEE shaping times: 0.5 ps, 1.0 ps, 2.0 ps, and 4.0 ps; three SNR: 20, 30, 100; and three sensor irradiation levels: pre-radiation, 5×10^{14} n/cm^2, and 1×10^{15} n/cm^2. For every point in this scan we evaluate the time resolution for LE and CF. Our results are a guideline on what time resolution can be achieved for a particular combination of analog bandwidth, SNR, and sensor.

The paper is organized as follows: the simulation is described in Sec. 2; algorithms used in the timing reconstruction and analysis are described in Sec. 3; simulation results are presented in Sec. 4, followed by the conclusion in Sec. 5.

2. Simulation Framework

Unprocessed signal pulses from the LGAD sensors are obtained from Weightfield2 (WF2), a 2-dimensional silicon simulator [4]. WF2 was used to simulate sets of 1000 signal pulses modeling the response of minimum-ionizing particles (MIP) traversing the LGAD sensor. Three sets of such signal pulses were generated for a 50 μm LGAD sensor at different levels of sensor irradiation: pre-irradiation, and after neutron fluences of 5×10^{14} n/cm^2 and 1×10^{15} n/cm^2. Gaussian white noise are added to these unprocessed signals, and the combined waveform is fed into the simulation of the FEE, illustrated in Fig. 1 and described in further detail in Sec. 2.1. The output of the FEE simulation is the convolution of the impulse response function and the input signal at the FEE. We consider four shaping constants for the impulse response of the FEE: 0.5, 1.0, 2.0, and 4.0 ns. At the output of the FEE block, we obtain simulated processed LGAD pulses, which include the effects of sensor fluctuations, the shaping of the FEE, and noise. The resulting processed pulses are scaled such that the landau-peak for each simulated condition is 50 mV, this choice does not affect the results and it is made such that the analysis downstream is invariant. A waveform analysis is performed with the pulses obtained at the output of the FEE block. We assign timestamps to each pulse by using algorithms that emulate ideal LE and CF discriminators. For each threshold we obtain an LE and CF timestamp as well as the corresponding time-over-theshold (ToT) of the pulse. The SNR is defined as the ratio of the most probable value (MPV) of the amplitude distribution to the width of the amplitude distribution at a fixed sample of noise-only waveforms. We study three SNR scenarios: 20, 30, and 100. A schematic diagram of the simulation is shown in Fig. 1.

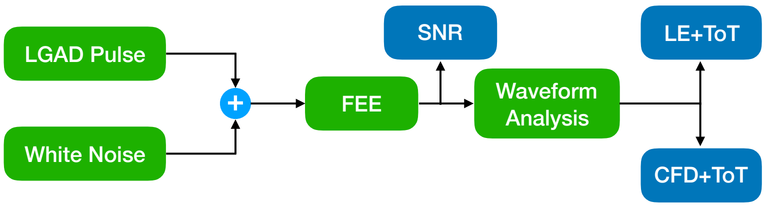

Figure 1: A schematic diagram of the simulation. Each simulation configurable block is shown in green. The most relevant outputs of the simulation are shown in blue.

2.1. Front-end electronics and noise injection

The front-end simulation combines analytical calculations and numerical methods. We implement two independent simulations, one based on the time domain and the other on the Laplace domain. Both simulation use as input the unprocessed WF2 LGAD pulses. The results of the two simulations are in agreement within statistical uncertainties and provide a cross check of the results. Sections 2.1.1 and 2.1.2 describe the details of the implementation of the front-end and noise simulation.

2.1.1. Front-end simulation

The front-end simulation is based on a single amplification stage. We focus on the BW of such an amplifier rather than variations thereof. The FEE is a second order low-pass filter with transfer function ($H(S)$) and impulse response ($h(t)$) given by equations 1 and 2, respectively.

$$H(S) = \frac{\frac{1}{\tau_s^2}}{(S + 1/\tau_s)^2} \qquad (1)$$

$$h(t) = \frac{t}{\tau_s^2} e^{-t/\tau_s} \qquad (2)$$

The output pulse of the FEE is the convolution (in time domain) of the unprocessed LGAD signal pulse from WF2 and the FEE impulse response function, given in Eq. 2. The time base for the pulses and the convolution is 10 ps, and we use this sampling time throughout the simulation. As stated above we focus the study on the BW of the FEE and to that end we scan the τ_s paremeter in Eq. 2 in the following set:$\{0.5, 1, 2, 4\}$ ns. This parameter is hereafter referred to as shaping time (ST). Figure 2 (left) shows the comparison of the impulse and LGAD responses for a ST of 1 ns while Figure 2 (right)

ST (ns)	0.5	1.0	2.0	4.0
Risetime (ns)	0.67 ± 0.02	0.86 ± 0.02	1.36 ± 0.02	2.48 ± 0.02

Table 1: Measured risetime for all shaping times studied: {0.5, 1, 2, 4} ns. Risetime is the 10% − 90% time difference as measured by the CFD algorithm described in Sec. 3.1. The uncertainty is the rms of the risetime distribution.

shows the LGAD response for all STs studied. We observe that the LGAD response is delayed with respect to the impulse response, and that pulse slew rate is decreased in the first nanosecond of the pulse. As expected, we also observe that the pulse risetime scale up with the ST and that the decay time is dominated by the ST. The measured risetimes (10% to 90%) are shown in Tab. 2.1.1.

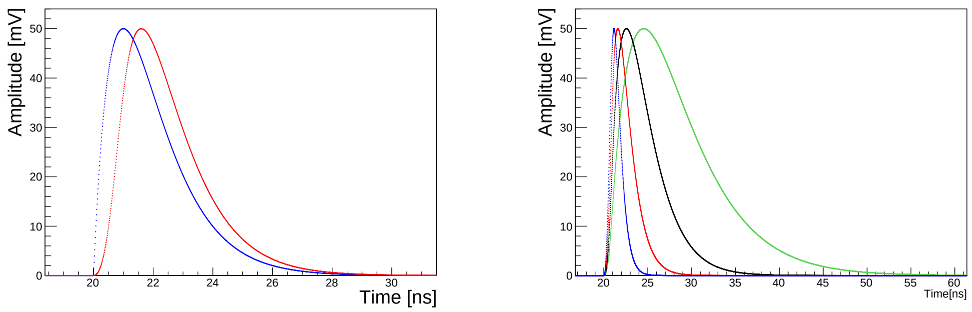

Figure 2: (Left) Comparison of impulse and LGAD reponses for the a shaping time (ST) of 1 ns. (Right) LGAD response for the four shaping times studied: {0.5, 1, 2, 4} ns. All pulses have been nomalized to achive a peak amplitude of 50 mV. Legends for the shaping times are shown in the plots.

2.1.2. Noise injection

Gaussian white noise is simulated by sampling the full time window (0 - 100 ns) in 10 ps intervals. Each sampled time is assign a random amplitude which is drawn from a gaussian distribution with zero mean and width corresponding to the SNR under study. It is important to note that the width of the gausian parameter is not exactly the SNR and needs to be adjusted depending on the ST of the FEE. The left panel of Figure 3 shows the gaussian white noise before and after a 1 ns FEE. The expected behavior for the noise is observed. The left panel of Figure 3 shows the output of the FEE block, with a 1 ns ST, for a pre-irradiated LGAD pulse after noise has been injected. The injected noise is such that the SNR is 30. SNR is defined ratio of the landau peak (the most probable value or MPV) of the pulse height distribution to the the r.m.s of the 100th sample over an ensemble of 1000 pulses.

3. Timing Reconstruction and Analysis

The time reconstruction is based on waveform analysis. We generate an ensamble of 1000 pulses sampled every 10 ps. Each pulse is interpolated using the Whittaker-Shannon

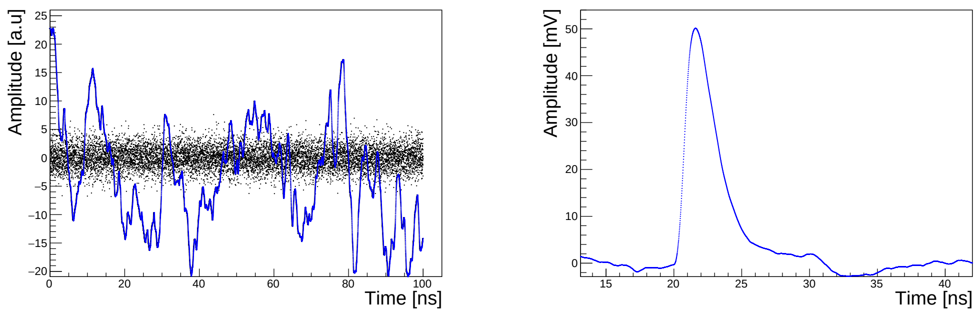

Figure 3: (Left) Comparison of gaussian white noise before and after the FEE. (Right) Example pulse at the output of the FEE block with a SNR of 30. Both figure use a shaping time (ST) of 1 ns. Legends for the shaping times are shown in the plots.

formula (sin(x)/x). Using the interpolated pulse we assign a timestamp by finding when a given voltage threshold has been crossed. The threshold can be a constant value (LE) or a constant fraction of the pulse height (CF). In the case of the CFD we also simulate more *realistic* implementations:split-and-delay as well as asecond order RC filter (Greg, please check naming). More details about the algorithms are given in Sec. 3.1. The time resolution is estimated by the width parameter of a gaussian fit to the timestamps obtained for a particular theshold. We apply a time-walk correction based on the time-over-threshold of the pulse. We note that this correction has a large improvement on the time resolution measured using the LE algorithm while the CF algorithm is mostly insentive to this correction, as seen in Fig. 4. Details about this correction are covered in Sec. 3.2. The timestamps are measured with a 20 ps binning while the time-over-thershold is measured with a 100 ps binning in order to simulate the effect of time quantization. We scan the LE and CF threshold such that we find the one with the lowest jitter.

3.1. Leading edge and constant fraction discriminators

The leading edge and constant fraction discriminator algorithms are *ideal* in the sense that they don't simulate the effect of electronics in a real implementation. Our approach is to sample the pulses every 10 ps and subsequently interpolate them using the Whittaker-Shannon formula (sin(x)/x) to more accurately determine the threshold crossing. In the LE case the theshold is scanned from 3–60 mV, while the CFD is scanned from 5–90 % of the current pulse maximum amplitude. For each thershold we obtain two timestamps: when the pulse first crosses the threshold (t_0) and when it crosses the second time (t_1), now in the opposite direction. The time-over-threshold is defined as the difference of the two timestamps (ToT $= t_1 - t_0$). The first timestamp, t_0, is used to determine the time resolution at given threshold. The time resolution is defined as the width of a gaussian fit to the t_0 distribution binned with a bin-width of 20 ps. The time resolution is obtained in two cases: before and after a time-walk correction. The time-walk correction aims to correct the known effect of time drift as a function of the pulse height. The time-walk correction removes this time drift and ensures that the time response is flat as a function of the pulse height. It is explained in greater detail in Sec. 3.2. Figure 4 shows the time resolution as a function of the threshold required for a pre-irradiated LGAD sensor with a ST of 1 ns and a SNR of 30. We note that the effect of the time-walk correction is large for LE and almost negligible for CF. Fig. 5 shows a typical t_0 distribution, using the LE and CF algorithms, for the pre-irradiated LGAD sensor after the ToT correction has been applied. The time resolution (σ_t) is measured to be 37.3 ± 1.4 and 33.0 ± 1.4 for the LE and CF, respectively. Additionally, we study more *realistic* CFD implementations: split-and-delay as well as a second order RC filter (Greg, please check naming) (see Sec. 3.1.1). We observe that *ideal* and split-and delay CFD implementations yield equivalent results within uncertainties. The second order RC filter shows a degradation on performance with respect to the split-and-delay implementation.

3.1.1. constant fraction discriminator implementations

GREG: PLEASE ADD TEXT HERE, I called the two implementations split-and-delay and second order RC previousluy in the text (also in red).

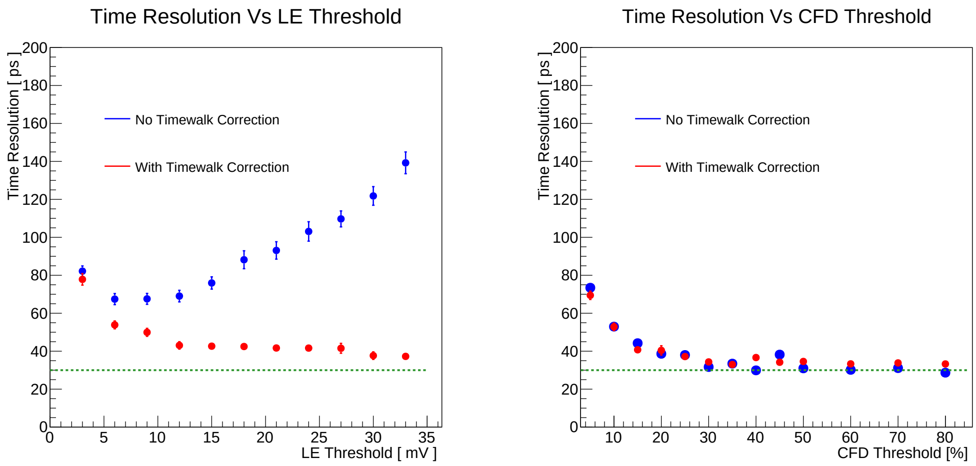

Figure 4: (Left) LE time resolution as a function of threshold. (Right) CF time resolution as a function of threshold. Both figure use pre-irradiated LGAD sensor with a ST of 1 ns and a SNR of 30.

3.2. Time-walk correction and time-over-threshold

A time-walk correction is applied in order to correct the timestamp drift of pulses with varying amplitudes. The correction is based on the measured time-over-theshold: $\mathrm{ToT} = t_1 - t_0$. As expected, we observe that the ToT correction is large for the LE case and negligible for CF (see Fig. 4). Figure 6 (left) shows a typical two dimensional map of t_0 and ToT for the LE algorithm, wherein a clear correlation between t_0 and ToT is observed. The time-walk correction is obtain by measuring the average t_0 in each ToT bin and subsequently fitting a 2nd-order polinomial (see Fig. 6 (right)). The resulting analytical expression after the fit is then used to correct and flatten the dependence of t_0 on ToT. The time-walk correction is expressed in Eq. 3, where p_2 and p_1 are the quadratic and linear coefficients of the 2nd-oder polynomial fit. Different corrections are derived for each simulation scenario characterized by the values of the simulation parameters: ST, SNR, and LGAD irradiation level. As shown in Fig. 4 (left) the effect of the time-walk

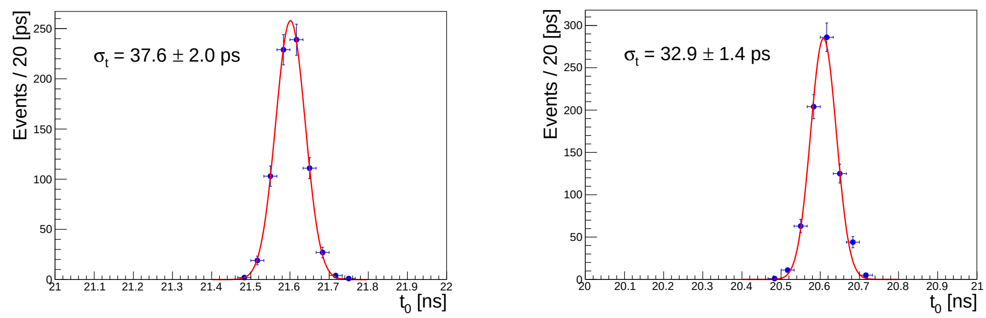

Figure 5: (Left) timestamp (t_0) distribution for a 30 mV threshold using a leading edge discriminator. (Left) timestamp (t_0) distribution for a 35% threshold using a constant fraction discriminator. Both figures include the time-walk correction based on the measured ToT. Both figures use a shaping time (ST) of 1 ns and correspond to SNR of 30.

dependes on the threshold used and correcting for it can yield significant improvements in the measured time resolution.

$$t_0 = t_0 - (p_2 \mathrm{ToT}^2 + p_1 \mathrm{ToT}) \tag{3}$$

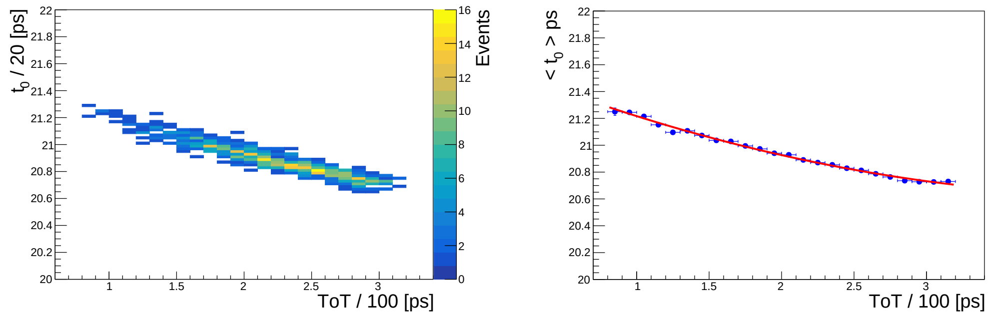

Figure 6: (Left) two dimenasional map of the timestamp (t_0) and ToT ($t_1 - t_0$). (Right) one dimensional projection of the timestamp (t_0) dependence on ToT, the red curve is the 2nd-order polinomial fit that ultimately is used to correct t_0. Both figures use a shaping time (ST) of 1 ns and correspond to a SNR of 30.

4. LGAD Front-end Electronics Performance

Herein we present a number of studies for a 50 μm LGAD. We study the time resolution as a function of irradiation for three different scenarios: pre-radiation, and after neutron fluences of 5×10^{14} n/cm^2 and 1×10^{15} n/cm^2. We also quantify the effect of the BW of the FEE by varying the the ST (τ_s), four STs are considerd: 0.5, 1, 2, and 4 ns. Additionally, we study the effect of noise by varying the SNR in all the scenarios described above. We consider three SNRs: 20, 30, and 100. Sec. 4.1 summarizes the effects of the shaping time and SNR, and and Sec. 4.2 summarizes the effect of irradiation.

	Time Resolution (ps)					
	Leading Edge			Constant Franction		
ST (ns)	SNR = 20	SNR = 30	SNR = 100	SNR = 20	SNR = 30	SNR = 100
0.5	38.4 ± 2.1	34.9 ± 1.7	28.8 ± 1.0	37.2 ± 1.9	34.5 ± 1.6	29.8 ± 1.9
1.0	45.4 ± 2.2	37.3 ± 1.4	28.7 ± 1.7	36.4 ± 1.8	33.0 ± 1.4	25.9 ± 1.3
2.0	63.4 ± 2.5	47.6 ± 2.0	30.7 ± 1.2	47.6 ± 1.9	34.3 ± 1.6	28.7 ± 1.7
4.0	103.0 ± 4.1	75.3 ± 2.8	37.6 ± 2.0	73.8 ± 3.1	54.8 ± 2.1	32.1 ± 1.3

Table 2: 50 μm pre-radiation LGAD sensor simulation: summary of best time resolution obtained for SNRs of 20, 30, and 100. Leading edge and constant fraction results are shown.

	Time Resolution (ps)		
	$(\mathrm{RC})^2$ Constant Fraction		
ST (ns)	SNR = 20	SNR = 30	SNR = 100
2.0	$68.0 \pm xx$	$xx \pm xx$	$xx \pm xx$

Table 3: 50 μm pre-radiation LGAD sensor using a second order RC implementation of a CFD. Summary of best time resolution obtained using a ST of 2ns for SNRs of 20, 30, and 100.

4.1. Front-end electronics shaping time and SNR studies

We scan the ST of the FEE and the SNR. The results for the pre-irradiated LGAD sensor are summarized in Table. 4.1, where the CF results are from the *ideal* implementation. The split-and-delay and the *ideal* CFD implementations are compatible within uncertainties thus we only use one table for those results. We observe that the best results are consistently obtained by the 0.5 ns and 1.0 ns STs regardless of the SNR. We observe that longer STs are more affected by less favorable SNR. For example, for an SNR of 20, the time resolution is 37 ps and 100 ps for a ST of 0.5 ns and 4.0 ns, respectively. We note that CF consistently outperforms LE, and this effect is also observed for less favorable SNR and slower ST. Comparing CF and LE for the 1.0 ns ST with SNR of 20 yields a difference in performance of 26 ps (when subtrated in quadrature). Additionally, we observe that time resolutions better than 25 ps could not be achieved which is consistent with the known intrinsic jitter of the LGAD sensor. The latter is taken into account by the WF2 simulation and confirmed in our study. For a SNR of 1000, essentially with zero noise, we obtained a time resolution consistent with 25 ps. Finally, in the case of the pre-irradiated sensor we observed that time resolutions of 35 ps are achievable for STs between 0.5 - 1.0 ns and a SNR of 30.

The second order RC CFD implementation shows a degradation on the time resolution when compared to the split-and-delay. Table. 4.1 shows the time resolution for the three SNR scenarios studied for a 2 ns ST. We observe a 50 ps degradation for a SNR of 20 and xx ps degradation for a SNR of 100.

4.2. Timing performace as a function of irradiation

We study the effect of irradiation on the time resolution of a 50 μm LGAD sensor. The impact of irradiation on the unprocessed signal pulse shapes are accounted for by the WF2 simulation. We consider three cases: pre-irradiated, and neutron fluences of 5×10^{14} n/cm^2 and 1×10^{15} n/cm^2. We perform the same studies as in the pre-irradiated

	Time Resolution (ps)					
	Leading Edge			Constant Franction		
ST (ns)	SNR = 20	SNR = 30	SNR = 100	SNR = 20	SNR = 30	SNR = 100
0.5	36.8 ± 1.9	32.0 ± 1.3	26.0 ± 1.2	32.5 ± 1.4	30.6 ± 1.2	25.1 ± 1.2
1.0	40.9 ± 1.4	33.8 ± 1.1	29.2 ± 1.0	33.4 ± 1.5	30.9 ± 0.9	26.1 ± 1.3
2.0	56.9 ± 2.4	45.3 ± 2.2	30.1 ± 1.1	43.7 ± 1.6	36.9 ± 1.3	24.4 ± 1.0
4.0	93.3 ± 3.6	67.9 ± 2.5	36.5 ± 1.3	70.8 ± 2.8	52.4 ± 1.9	29.9 ± 1.9

Table 4: 50 μm LGAD sensor simulation after neutron fluence of 5×10^{14} n/cm^2: summary of best time resolution obtained for SNRs of 20, 30, and 100. Leading edge and constant fraction results are shown.

	Time Resolution (ps)					
	Leading Edge			Constant Franction		
ST (ns)	SNR = 20	SNR = 30	SNR = 100	SNR = 20	SNR = 30	SNR = 100
0.5	47.8 ± 2.0	37.6 ± 2.0	26.6 ± 1.3	41.9 ± 1.9	34.3 ± 1.1	24.1 ± 1.0
1.0	59.9 ± 2.3	46.8 ± 1.8	28.1 ± 1.5	46.5 ± 1.9	36.8 ± 1.3	23.1 ± 0.9
2.0	89.7 ± 3.5	68.2 ± 2.6	32.3 ± 1.4	64.7 ± 2.8	49.6 ± 2.1	27.3 ± 0.9
4.0	147.3 ± 5.1	109.0 ± 4.3	42.6 ± 1.9	118.6 ± 4.0	84.1 ± 3.2	33.8 ± 1.1

Table 5: 50 μm LGAD sensor simulation after neutron fluence of 1×10^{15} n/cm^2: summary of best time resolution obtained for SNRs of 20, 30, and 100. Leading edge and constant fraction results are shown.

case discussed in Sec. 4.1. The results for the irradiated LGAD are presented in Tab. 4.1 and Tab. 4.1 for neutron fluences of 5×10^{14} n/cm^2 and 1×10^{15} n/cm^2, respectively. We observe similar trends to those of the pre-radiation sensor described in Sec. 4.1. We note that when using STs between 0.5 - 1.0 ns and a SNR of 30, time resolutions of the order of 31 ps and 37 ps are obtained for 5×10^{14} n/cm^2 and 1×10^{15} n/cm^2, respectively.

5. Conclusion

We study the time resolution of a 50 μm LGAD sensor using a simulation framework that includes the modeling of the raw unprocessed LGAD signal pulse, the front-end electronics, and the quantization. We focus on the shaping time and sigal-to-noise ratio of the front-end electronics and its interplay with the irradiation level of the sensor. We reproduce the known LGAD jitter of 25 ps for fast STs and large SNRs. We observe a clear degradation of the time resolution with SNR and slower STs. The best results are obtained using a ST of 0.5 ns and using CF discriminator, and similar results are obtained with a ST of 1.0 ns. For a SNR of 30 and for STs betwen 0.5-1.0 ns we obtain time resoutions between 30 - 37 ps for the 3 irradiations considered. The reduction in gain with irradiation could bring the SNR for the most irradiated LGAD (1×10^{15} n/cm^2) to 20 and thus worsen the time resolution to 42 - 47 ps. We note a clear gain in performace of CF over LE discriminators, particularly at low SNR and the largest irradiation level. For an ST of 1.0 ns at SNR = 30, the performance improvement of CF over LE is 26ps for the pre-irradiated sensor and 37ps for the irradiated sensor with neutron fluence of 1×10^{15} n/cm^2. A performance degradiation is observed when using a second order RC implementation of the CFD, specially at lower SNRs. Overall our simulation results indicate that time resolutions better than 45 ps are achievable for a 50 μm LGADs for irradiation levels up to neutron fluences of 1×10^{15} n/cm^2.

Acknowledgment

A. Apresyan gratefully acknowledges support from DOE Early Career Research Program.

This document was prepared using the resources of the Fermi National Accelerator Laboratory (Fermilab), a U.S. Department of Energy, Office of Science, HEP User Facility. Fermilab is managed by Fermi Research Alliance, LLC (FRA), acting under Contract No. DE-AC02-07CH11359. Part of this work was performed within the framework of the CERN RD50 collaboration.

This work was supported by the Fermilab LDRD 2017.027; by the United States Department of Energy grant DE-FG02-04ER41286; by the California Institute of Technology High Energy Physics under Contract DE-SC0011925; by the European Union's Horizon 2020 Research and Innovation funding program, under Grant Agreement no. 654168 (AIDA-2020) and Grant Agreement no. 669529 (ERC UFSD669529); by the Italian Ministero degli Affari Esteri and INFN Gruppo V; and by the Spanish Ministry of Economy, Industry and Competitiveness through the Particle Physics National Program (ref. FPA2014-55295-C3-2-R and FPA2015-69260-C3-3-R) co-financed with FEDER funds.

References

[1] A. Apresyan, S. Xie, C. Pena, *et al.*, "Studies of Uniformity of 50 μm Low-Gain Avalanche Detectors at the Fermilab Test Beam," *Nucl. Instrum. Meth.*, vol. A895, pp. 158–172, 2018.

[2] N. Cartiglia *et al.*, "Beam test results of a 16 ps timing system based on ultra-fast silicon detectors," *Nucl. Instrum. Meth. A*, vol. 850, pp. 83 – 88, 2017.

[3] G. Pellegrini, P. Fernández-Martinez, M. Baselga, C. Fleta, D. Flores, V. Greco, S. Hidalgo, I. Mandić, G. Kramberger, D. Quirion, and M. Ullan, "Technology developments and first measurements of Low Gain Avalanche Detectors (LGAD) for high energy physics applications," *Nuclear Instruments and Methods in Physics Research Section A: Accelerators, Spectrometers, Detectors and Associated Equipment*, vol. 765, pp. 12 – 16, 2014. HSTD-9 2013 - Proceedings of the 9th International.

[4] H. F. W. Sadrozinski, A. Seiden, and N. Cartiglia, "4D tracking with ultra-fast silicon detectors," *Rept. Prog. Phys.*, vol. 81, no. 2, p. 026101, 2018.